JB
Journals.ASM.org

Enzymology and Structure of the GH13_31 Glucan 1,6-α-Glucosidase That Confers Isomaltooligosaccharide Utilization in the Probiotic *Lactobacillus acidophilus* NCFM

Marie S. Møller,[a] Folmer Fredslund,[a]* Avishek Majumder,[a]* Hiroyuki Nakai,[a]* Jens-Christian N. Poulsen,[b] Leila Lo Leggio,[b] Birte Svensson,[a] and Maher Abou Hachem[a]

Enzyme and Protein Chemistry, Department of Systems Biology, Technical University of Denmark, Kongens Lyngby, Denmark,[a] and Biophysical Chemistry Group, Department of Chemistry, University of Copenhagen, Copenhagen, Denmark[b]

Isomaltooligosaccharides (IMO) have been suggested as promising prebiotics that stimulate the growth of probiotic bacteria. Genomes of probiotic lactobacilli from the acidophilus group, as represented by *Lactobacillus acidophilus* NCFM, encode α-1,6 glucosidases of the family GH13_31 (glycoside hydrolase family 13 subfamily 31) that confer degradation of IMO. These genes reside frequently within maltooligosaccharide utilization operons, which include an ATP-binding cassette transporter and α-glucan active enzymes, e.g., maltogenic amylases and maltose phosphorylases, and they also occur separated from any carbohydrate transport or catabolism genes on the genomes of some acidophilus complex members, as in *L. acidophilus* NCFM. Besides the isolated locus encoding a GH13_31 enzyme, the ABC transporter and another GH13 in the maltooligosaccharide operon were induced in response to IMO or maltotetraose, as determined by reverse transcription-PCR (RT-PCR) transcriptional analysis, suggesting coregulation of α-1,6- and α-1,4-glucooligosaccharide utilization loci in *L. acidophilus* NCFM. The *L. acidophilus* NCFM GH13_31 (*La*GH13_31) was produced recombinantly and shown to be a glucan 1,6-α-glucosidase active on IMO and dextran and product-inhibited by glucose. The catalytic efficiency of *La*GH13_31 on dextran and the dextran/panose (trisaccharide) efficiency ratio were the highest reported for this class of enzymes, suggesting higher affinity at distal substrate binding sites. The crystal structure of *La*GH13_31 was determined to a resolution of 2.05 Å and revealed additional substrate contacts at the +2 subsite in *La*GH13_31 compared to the GH13_31 from *Streptococcus mutans* (*Sm*GH13_31), providing a possible structural rationale to the relatively high affinity for dextran. A comprehensive phylogenetic and activity motif analysis mapped IMO utilization enzymes from gut microbiota to rationalize preferential utilization of IMO by gut residents.

Increasing attention is currently aimed at understanding the molecular basis by which probiotic bacteria, mainly belonging to the *Bifidobacterium* and *Lactobacillus* genera, confer their well-documented positive health effects (37, 53). Utilization of oligosaccharides, not otherwise digestible by human enzymes, has been recognized as an important attribute of probiotics (5, 15, 28, 37). Only a few oligosaccharides such as fructooligosaccharides (FOS) or β-linked galactooligosaccharides (GOS) are well established as prebiotics that selectively stimulate the growth and/or activities of probiotic bacteria (11). Commercial preparations of isomaltooligosaccharides (IMO), typically including panose [α-D-Glc*p*(1–6)-α-D-Glc*p*(1–4)-D-Glc*p*], are potential prebiotics as humans and monogastric animals lack IMO-hydrolyzing enzymes except for the sucrase-isomaltase complex active on isomaltose (IG2) (22, 24, 29, 32, 49). This is consistent with the bifidogenic effect of IMO in the human gut (17, 23) and increased lactobacillus numbers in rats due to IMO intake (25, 43). Remarkably, utilization of IMO by human gut bacteria and especially lactobacilli is largely unexplored on the enzymatic level as no IMO-degrading enzymes from a probiotic have been characterized to date. By comparison, Gram-positive bacteria from the *Streptococcus* and *Bacillus* genera are known to produce 1,6-α-glucosidases active on IMO and in some cases also on dextran (α-1,6-linked glucan) (43, 47, 54, 55). These enzymes hydrolyze α-1,6-glycosidic linkages at the nonreducing end with retention of anomeric configuration (EC 3.2.1.10) and belong to glycoside hydrolase family 13 subfamily 31 (GH13_31) (46) according to the CAZy database classification (http://www.cazy.org/), which assigns carbohydrate-active enzymes into GH families sharing structural fold and stereochemical mechanisms (8) (sequence- and structure-related families are further classified into clans). GH13_31 harbors isomaltulose synthases (EC 5.4.99.11) and α-glucosidases. The latter are divided into two specificities based on substrate size preference: (i) glucan 1,6-α-glucosidases (G16G) preferring IMO longer than IG2 and active on dextran and (ii) oligo-1,6-α-glucosidases (O16G) inactive on dextran and preferring shorter IMO with highest activity on IG2. Both types of enzymes are highly regioselective, showing little or no activity toward glucosidic linkages other than α-1,6 (43, 47, 54, 55). The only biochemically and structurally characterized GH13_31 with a glucan 1,6-α-glucosidase specificity (G16G) is from *Streptococcus mutans* (*Sm*GH13_31) (19, 43). By comparison, the biochemical properties of three GH13_31 oligo-1,6-α-glucosidases (O16Gs) from *Bacillus thermoglucosidasius*

Received 13 April 2012 Accepted 29 May 2012
Published ahead of print 8 June 2012
Address correspondence to Maher Abou Hachem, maha@bio.dtu.dk.
* Present address: Folmer Fredslund, MAX-lab, Lund University, Lund, Sweden; Avishek Majumder, Einar Willumsen A/S, Broendby, Denmark; Hiroyuki Nakai, Food Glycoscience Laboratory, Niigata University Graduate School of Science and Technology, Nishiku, Niigata, Japan.
Supplemental material for this article may be found at http://jb.asm.org/.

doi:10.1128/JB.00622-12

(*Geobacillus thermoglucosidasius*), *Bacillus coagulans*, and *Bacillus cereus* have been reported, and the structure of the last enzyme has been determined (43, 47, 54, 55).

Lactobacillus acidophilus NCFM is a commercially important probiotic isolated from the human gut and characterized in the 1970s (16). It has since then been widely investigated for its physiological, biochemical, genetic, and fermentative properties (44). The numerous proteins related to carbohydrate transport and metabolism encoded by *L. acidophilus* NCFM reflect its capacity to utilize a variety of mono-, di-, oligo-, and polysaccharides (3). Notably, panose was shown to sustain the growth of *L. acidophilus* NCFM *in vitro* (32), in line with the suggested prebiotic effect of IMO.

In the present study, the catabolism of IMO is examined in *L. acidophilus* NCFM as a model organism for probiotic lactobacilli from the gut niche. Genome analysis confirmed the presence of a putative GH13_31 G16G-encoding gene that likely confers IMO hydrolysis. This gene was heterologously expressed in *Escherichia coli*, and the recombinant enzyme, designated *L. acidophilus* GH13_31 (*La*GH13_31), was biochemically and structurally characterized. Furthermore, an analysis was performed to map IMO utilization loci in probiotic lactobacilli, highlighting commonalities and differences in the organization of IMO utilization genes on the genomes of this group of organisms important for human health.

MATERIALS AND METHODS

High-purity chemicals and commercial enzymes were from Sigma-Aldrich, St. Louis, MO, unless otherwise stated. The commercial IMO mix was from Wako Pure Chemical Industries, Osaka, Japan.

Bioinformatic analysis. For the sequence alignment, the first 100 protein sequences from BLASTP searches using LBA0264 and LBA1872 were retrieved and complemented with lactobacillus sequences from CAZy (8) annotated as GH13_31. Sequences with >95% identity were removed using Skipredundant from the EMBOSS software suite (40). The resulting set of sequences was aligned using the program MUSCLE (12), and a neighbor-joining tree was constructed with 1,000 bootstrap steps using Clustal W, version 2.0 (27), and visualized by aid of Dendroscope (20) and Inkscape (http://inkscape.org). The organization of O16G- and G16G-encoding genes from various organisms was investigated using the genome database provided by the National Center for Biotechnology Information (NCBI), U.S. National Library of Medicine (http://www.ncbi.nlm.nih.gov/genomes/lproks.cgi).

Purification of IMO and semiquantitative RT-PCR. In order to verify the functionality of the genes predicted to be involved in IMO utilization, *L. acidophilus* NCFM was grown on purified IMO from a commercial mix first treated with rice α-glucosidase to hydrolyze maltooligosaccharides into glucose. The hydrolysate was ultrafiltered (10-kDa Amicon filter; Millipore, Billerica, MA), desalted (Amberlite MB-20; Fluka, Sigma-Aldrich), and filtered (0.45-μm pore size; Frisenette Aps, Knebel, Denmark). Glucose was removed by a high-performance liquid chromatograph ([HPLC] UltiMate 3000; Dionex, Sunnyvale, CA) equipped with a refractive index detector (RI-101; Showa Denko, Kanagawa, Japan) using a TSKgel Amide-80 column (5-μm particle size; 4.6 by 250 mm with 4.6- by 10-mm guard column [Tosoh, Tokyo, Japan]) at a constant flow rate 1 ml/min of mobile phase (acetonitrile-water, 70:30 [vol/vol]) at 70°C. The purity was confirmed based on peaks detected with high-performance anion exchange chromatography with peramperometric detection ([HPAEC-PAD] ICS-3000; Dionex) on a CarboPac PA200 anion exchange column (3 by 250 mm and 3- by 50-mm guard column; Dionex) eluted by a linear 0 to 125 mM sodium acetate gradient in 100 mM NaOH (for 35 min at 25°C; flow rate, 0.35 ml/min). The IMO components were identified based on standards: IG2, isomaltotriose (IG3), isomaltotetraose (IG4), isomaltopentaose (IG5), panose, glucose, and maltooligosaccharides from maltose through to maltoheptaose. The purified IMO were essentially glucose free and contained IMO having degrees of polymerization of 2 to 4 (DP 2 to 4).

L. acidophilus NCFM was grown (in duplicate) with 1% of either glucose, maltotetraose, or IMO at DP 2 to 4 (purified as above), under aerobic conditions and without agitation at 37°C in a 40-ml batch culture in semiessential medium for lactic acid bacteria (5). The cells were harvested at late log phase (optical density at 600 nm [OD_{600}] of 0.85 for glucose and 0.3 for IMO and maltotetraose) by centrifugation (at 3,200 × *g* for 10 min at 4°C) and washed twice with 0.9% NaCl. Cell disintegration, total RNA preparation, and semiquantitative reverse transcription-PCR (RT-PCR) were carried out as previously described (31). PCR amplification was carried out with the primer pairs targeting LBA0264 (encoding *La*GH13_31) and genes in the maltooligosaccharide transport and catabolism gene cluster (LBA1866, LBA1867, and LBA1872) (34), and *L. acidophilus* NCFM 16S rRNA (LBA2071) transcripts, whose expression is always constant, were used as internal controls (see Table S1 in the supplemental material).

Cloning of LBA0264. *L. acidophilus* NCFM genomic DNA, prepared as previously described (34), was used as a template for PCR amplification of the gene encoding *La*GH13_31 (GenBank accession number AAV42157.1; locus tag number LBA0264), with forward primer 5′-C TA**GCTAGC**GCTTCATGGTGGAAAAATGCTGTTG-3′ and reverse primer 5′-CCG**CTCGAG**TTCAATTACTTTGCTTATGAAAGCCTC-3′. The PCR amplicon (1,632 bp), flanked by NcoI and XhoI restriction sites (in bold), was cloned into pET21a(+) (Novagen, Darmstadt, Germany) and transformed into *E. coli* TOP10 (Invitrogen, Carlsbad, CA) by heat shock. Transformants were selected on LB-agar plates with 100 μg ml^{-1} ampicillin, and positive transformants harboring pET-21a(+)-*La*GH13_31 were verified by restriction analysis and full sequencing. *E. coli* BL21(DE3) cells (Invitrogen) transformed with pET21a(+)-*La*GH13_31 were used to produce the enzyme.

Production and purification. *La*GH13_31 was produced in a 5-liter bioreactor (Biostat B; B. Braun Biotech International, Melsungen, Germany) according to a fed-batch protocol developed previously for production of other *L. acidophilus* NCFM recombinant enzymes (14), with the exception that the induction (OD_{600} of 8.3) was carried out at 16°C with 40 μM isopropyl-β-D-thiogalactopyranoside (IPTG). The fermentation was terminated after 23 h of induction, and 61 g of cell pellet (harvested by centrifugation at 12,200 × *g* for 10 min at 4°C) was resuspended in 60 ml of a buffer containing 10 mM HEPES, 10 mM imidazole, 10% glycerol, 0.5 M NaCl, and 2 mM $CaCl_2$ (pH 7.5) (buffer A) and disrupted by passage through a French press at 600 × 10^5 Pa. After Benzonase nuclease (Novagen) treatment, the suspension was centrifuged (at 43,000 × *g* for 65 min) and sterile filtered (0.22-μm pore size). *La*GH13_31 was purified by immobilized metal ion affinity chromatography using a 5-ml HisTrap HP column (GE Healthcare, Uppsala, Sweden) as described elsewhere (14). This purification step was followed by anion exchange chromatography using an 8-ml Mono Q 10/100 GL column (GE Healthcare) equilibrated in 10 mM HEPES, pH 7.0, and 2 mM $CaCl_2$ (GE Healthcare) and installed on an ÄKTAexplorer chromatograph (GE Healthcare). The *La*GH13_31-loaded column was stringently washed (60 ml/h, 0.25 M NaCl, 12 column volumes [CV]) and eluted at the same flow rate using a linear gradient (0.25 to 0.29 M NaCl, 15 CV; 0.29 to 0.5 M NaCl, 2 CV). The fractions containing activity were analyzed by SDS-PAGE, pooled, concentrated (10-kDa Amicon filter; Millipore), and buffer exchanged to 20 mM 2-(*N*-morpholino)ethanesulfonic acid (MES)-NaOH, pH 6.5, 2 mM $CaCl_2$, and 100 mM NaCl. The protein concentration was determined spectrophotometrically using the molar extinction coefficient ε_{280} of 138,180 M^{-1} cm^{-1} as determined by amino acid analysis (4). The isoelectric point (pI) was determined by focusing on a PhastGel IEF 4 to 6.5 isoelectric focusing gel and a pI marker (2.8 to 6.5) (GE Healthcare) using the PhastSystem (Pharmacia, Uppsala, Sweden).

Enzyme activity: standard enzyme assay. A standard assay (50 μl) was performed in 60 mM MES-NaOH, pH 6.0, 2 mM $CaCl_2$, and 0.005%

bovine serum albumin (BSA) using 2 mM *p*-nitrophenyl α-D-glucopyranoside (PNPG) as the substrate and enzyme (2.5 to 6 nM) for 10 min at 37°C. The reaction was stopped by addition of 1 M Na_2CO_3 (200 μl), and the A_{410} was measured. The concentration of liberated *p*-nitrophenol (PNP) was calculated from a PNP standard curve. One unit of enzyme activity (U) was defined as the amount of enzyme required to liberate 1 μmol of PNP per min under the assay conditions.

Optimum pH. The pH optimum of *La*GH13_31 (2.8 nM, 200 μl) was determined using the standard assay in 40 mM Britton-Robinson universal buffers pH 2 to 10 (7) and stopped by addition of 1 M Na_2CO_3 (800 μl).

Temperature optimum and stability. The temperature optimum of *La*GH13_31 activity was determined by performing the standard assay at pH 6.0 at 21 to 60°C. The rate of irreversible thermal inactivation was also determined at 37°C and 50°C by incubation of the enzyme (28.3 nM) and measurement of residual activity at eight time points (20-μl aliquots, immediately cooled on ice) using the standard assay. The inactivation rate constant k (min^{-1}) was calculated assuming first-order kinetics from the slope of $\ln(A_t/A_0)$ plotted against time (min), where A_t is the activity at time t (min) and A_0 is the initial activity; the half-life ($t_{1/2}$) was calculated from the equation $t_{1/2} = \ln(2)/k$.

Determination of kinetic parameters of IMO hydrolysis. Reaction mixtures (300 μl) containing *La*GH13_31 (1.4 to 9.8 nM) and PNPG (0.05 to 10 mM), IG2 (2.5 to 80 mM), IG3 (isomaltotriose, 1 to 25 mM), IG4 (isomaltotetraose, 2.5 to 30 mM), panose (0.5 to 14 mM), or dextran (1.6 to 40 mg/ml) were used to determine the initial hydrolysis rates by transferring aliquots (50 μl) into 1 M Na_2CO_3 (200 μl for PNPG) or 2 M Tris-HCl, pH 7.0 (100 μl for other substrates), at 4-min intervals for 16 min. Liberated PNP was measured as described above, whereas glucose liberated from other substrates was quantified by a modified glucose oxidase-peroxidase method (GOPOD) (Megazyme, Bray, Ireland), as follows. First, 200 μl of the GOPOD reagent was preheated for 5 min at 40°C, and then 100 μl of the stopped reaction sample was added. After 20 min at 40°C the A_{510} was measured. Inhibition kinetics of *La*GH13_31 by 6 or 8 mM glucose was probed using PNPG as the substrate as described above. The Michaelis-Menten model was fit to the initial rates to determine k_{cat} and K_m using Sigma plot, version 9.01 (SYSTAT Software, Inc., Richmond, CA) and also applied to determine the K_i for glucose inhibition.

Crystallization. The purified protein was concentrated to 16 mg/ml in 20 mM MES-NaOH buffer, pH 6.5, 100 mM NaCl, and 2 mM $CaCl_2$ as described above. Initial crystallization conditions were obtained by screening using an Oryx 8 Protein Crystallization Robot (Douglas Instruments, Ltd., United Kingdom) with 96-well trays at room temperature. A JCSG+ screen (Qiagen) was set up in sitting drops consisting of 1:1 (total, 200 nl) and 1:2 (total, 300 nl) protein/reservoir solutions, respectively. Small thin needles were obtained with a reservoir containing 20% glycerol, 16% polyethylene glycol 8000 (PEG 8000), and 0.1 M MES, pH 6.5, and were reproduced in 24-well VDX trays (Hampton Research) in sitting drops consisting of 2 μl of protein and 1 μl of reservoir solution. No extra cryoprotection was used before the crystals were mounted.

Data collection, processing, and refinement. A native data set was collected to 2.05-Å resolution at the I911-2 side station of the Cassiopeia beamline MAX-lab, Lund, Sweden. The space group was determined as $P2_12_12$ with the following cell dimensions: a = 55.8 Å, b = 107.3 Å, and c = 103.6 Å. Processing and scaling of the data were performed with XDS and XSCALE (21) (data shown in Table 1). Molecular replacement with MOLREP (51) using *Sm*GH13_31 (Protein Data Bank identification [PDB ID], 2ZIC) as a search model yielded a clear solution with one monomer in the asymmetric unit. The model was rebuilt using phenix.autobuild (50) and COOT (13) and refined with phenix.refine (2) to an R/R_{free} of 0.151/0.196. The final model includes *La*GH13_31 residues 2 to 538 (using the native protein numbering) in addition to eight glycerol molecules, three MES molecules (for MES residue 1547 in chain A, only the sulfonic acid moiety is modeled), 475 water molecules, and one calcium ion (Table 1). No electron density was observed for three N-terminal residues and the C-terminal His_6 tag (eight residues). No Ramachandran outliers were observed. A double conformation was modeled for Asn7, and Lys247 was truncated at the C^{β}-atom as the side chain collided with its symmetry mate. Protein coordinates were represented with PyMOL, version 1.4.1 (Schrödinger, LLC).

TABLE 1 Data collection and refinement statistics

Parameter[a]	Value for the parameter
Data collection	
Wavelength (Å)	1.038
High resolution (Å)	2.05
Space group	$P2_12_12$
Unit cell parameter (Å)	
a	55.8
b	107.3
c	103.6
No. of unique reflections	39,496
Resolution (Å)	30-2.05 (2.10-2.05)
Completeness (%)	97.2 (91.2)
Redundancy	5.3 (4.7)
Mean $I/\sigma(I)$	25.55 (9.7)
R_{sym} (%)	5.4 (20.8)
R_{rim} (%)	5.9 (23.1)
Refinement	
No. of protein atoms	4,431
No. of hetero atoms	77
No. of water molecules	475
R-factor (%)	13.7
R_{free} (%)	18.3
RMSD value from ideality	
Bond length (Å)	0.010
Bond angle (°)	1.24
Ramachandran plot (%)[b]	
Allowed	100
Favored	97.2
Outliers	0.0

[a] Data were collected using MAX-lab beamline I911-2. Values in parentheses are for the outer-resolution shell. RMSD, root mean square deviation.
[b] Calculated using MolProbity (9).

Protein structure accession number. Atomic coordinates of *La*GH13_31 have been deposited at the Protein Data Bank under accession code 4aie.

RESULTS

Bioinformatic analysis. Only a single gene (LBA0264) in the genome of *L. acidophilus* NCFM was annotated to encode a GH13_31 in CAZy. The amino acid sequence of LBA0264 showed highest identity to glucan 1,6-α-glucosidases (G16G) from streptococci (56 to 61%), followed by O16Gs from bacilli (49 to 53%), whereas clearly lower identities were shared with trehalose-6-phosphate hydrolases from *Bacillus subtilis* and *E. coli*, all of which are assigned into GH13 (Table 2). Another GH13 gene, LBA1872 (AAV43672.1), located within the maltooligosaccharide gene cluster (34), was not assigned into subfamily 31 but displayed lower primary structure identities of 30 to 37% to other characterized O16G and other α-glucosidases of GH13 (see Table S2 in the supplemental material). The identity between LBA0264 and LBA1872 is 35.4%. A multiple sequence alignment of top hits from BLASTP with LBA0264 and LBA1872 combined with *Sm*GH13_31, characterized O16Gs, and enzymes from lactobacilli assigned to GH13_31 showed that LBA0264 aligns very well with *Sm*GH13_31 in the conserved regions, which define pivotal ac-

TABLE 2 Amino acid sequence comparison of the gene product of LBA0264 to functionally characterized GH13 enzymes[a]

Enzyme and organism(s)	UniProtKB/Swiss-Prot accession no.	Identity (%)	Similarity (%)	Gap	Score	Reference(s)
Glucan-1,6-α-glucosidase						
Streptococcus mutans	Q99040[b]	57.6	75.0	2.0	1,697	19, 42, 43
Oligo-1,6-α-glucosidase						
Bacillus cereus	P21332[b]	53.1	70.1	4.5	1,585	48, 54, 56
Bacillus thermoglucosidasius (Geobacillus thermoglucosidasius)	P29094[b]	51.8	69.3	4.8	1,575	55
Bacillus coagulans	Q45101[c]	51.5	66.5	6.4	1,492	47
Trehalose-6-phosphate hydrolase						
Bacillus subtilis	P39795[d]	46.1	63.9	4.3	1,387	18
Escherichia coli K-12	P28904[d]	45.8	63.4	6.4	1,307	41

[a] The similarity of amino acid sequences was investigated using the BLASTP program (UniProtKB/Swiss-Prot database). The proteins are listed according to descending percentages of sequence identity and grouped according to specificity.
[b] GH13 subfamily 31.
[c] GH13, no subfamily.
[d] GH13 subfamily 29.

tive-site residues and region V (Fig. 1), which is the α-1,6 specificity motif in the α-amylase family (clan GH-H according to the CAZy classification) (38). In addition, LBA0264, like *Sm*GH13_31, has the shorter loop between conserved regions II and III, which defines the G16G subspecificity in GH13_31 (43). In contrast, LBA1872 lacked the α-1,6 specificity motif, suggesting that it might have another specificity. In the unrooted phylogenetic tree (Fig. 2) of the enzymes included in the multiple sequence alignment, LBA0264 clusters together with *Sm*GH13_31 and several putative G16Gs from lactobacilli, while LBA1872 segregates in a different cluster together with uncharacterized proteins from a wide range of lactobacilli (see Table S3 in the supplemental material for details). The characterized O16Gs from bacilli form a third cluster together with mainly uncharacterized sequences from bacilli and other Gram-positive bacteria, including a few *Lactobacillus* sequences, and this cluster is more closely related to the G16G group (Fig. 2). Thus, the analysis supports the annotation of LBA0264 as an IMO active enzyme, whereas LBA1872 seemed not to be involved in IMO hydrolysis based on this analysis.

Transcriptional analysis of genes possibly involved in IMO utilization. Both IMO and maltooligosaccharides sustained the growth of *L. acidophilus* NCFM, albeit to a lower cell density than glucose. The semiquantitative RT-PCR analysis showed the transcription of LBA0264 to be upregulated on both maltotetraose and the purified IMO mix compared to cells grown on glucose (Fig. 3). Similarly, LBA1872 and the permease (LBA1866) as well as the solute binding protein (LBA1867) components of the ATP-binding cassette (ABC) transport system in the maltooligosaccharide gene cluster were also upregulated on both maltotetraose and IMO.

Production and basic characterization of LBA0264, *La*GH13_31. *La*GH13_31 was purified to electrophoretic homo-

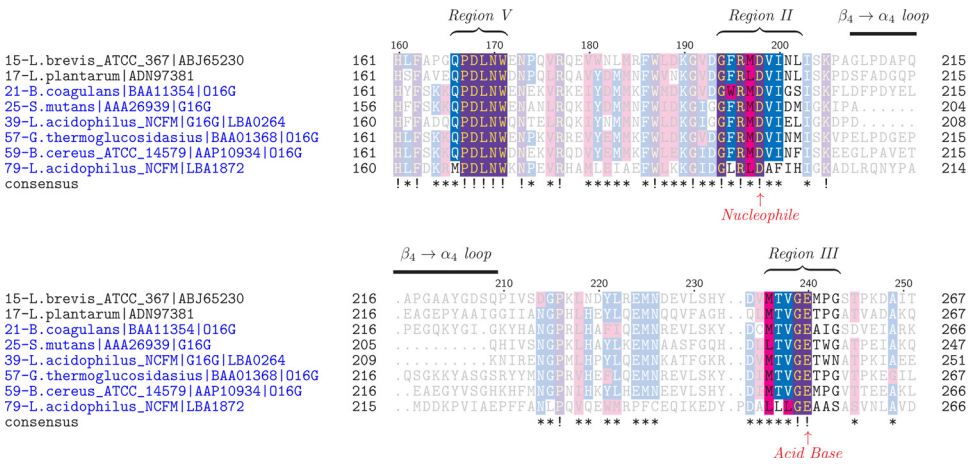

FIG 1 Excerpt of multiple sequence alignment of selected characterized GH13_31 enzymes and homologous sequences from BLASTP with LBA0264 as well as LBA1872. Regions II and III, conserved in α-amylase family enzymes, encompass the catalytic groups and certain pivotal active-site residues (30). Region V defines the specificity motifs of 1,6-α-glucosidases and neopullulanases (38). The catalytic residues are marked with arrows. The amino acid numbering on the top of the alignment corresponds to the glucan 1,6-α-glucosidase from *Lactobacillus acidophilus* NCFM (*La*GH13_31, LBA0264), and the protein sequences are numbered as in the full-alignment in Fig. S1 in the supplemental material and in Fig. 2. Similar residues are highlighted in pink; conserved residues are highlighted in blue (≥50% conserved) or purple (≥75% conserved). *L. brevis*, *Lactobacillus brevis*; *L. plantarum*, *Lactobacillus plantarum*.

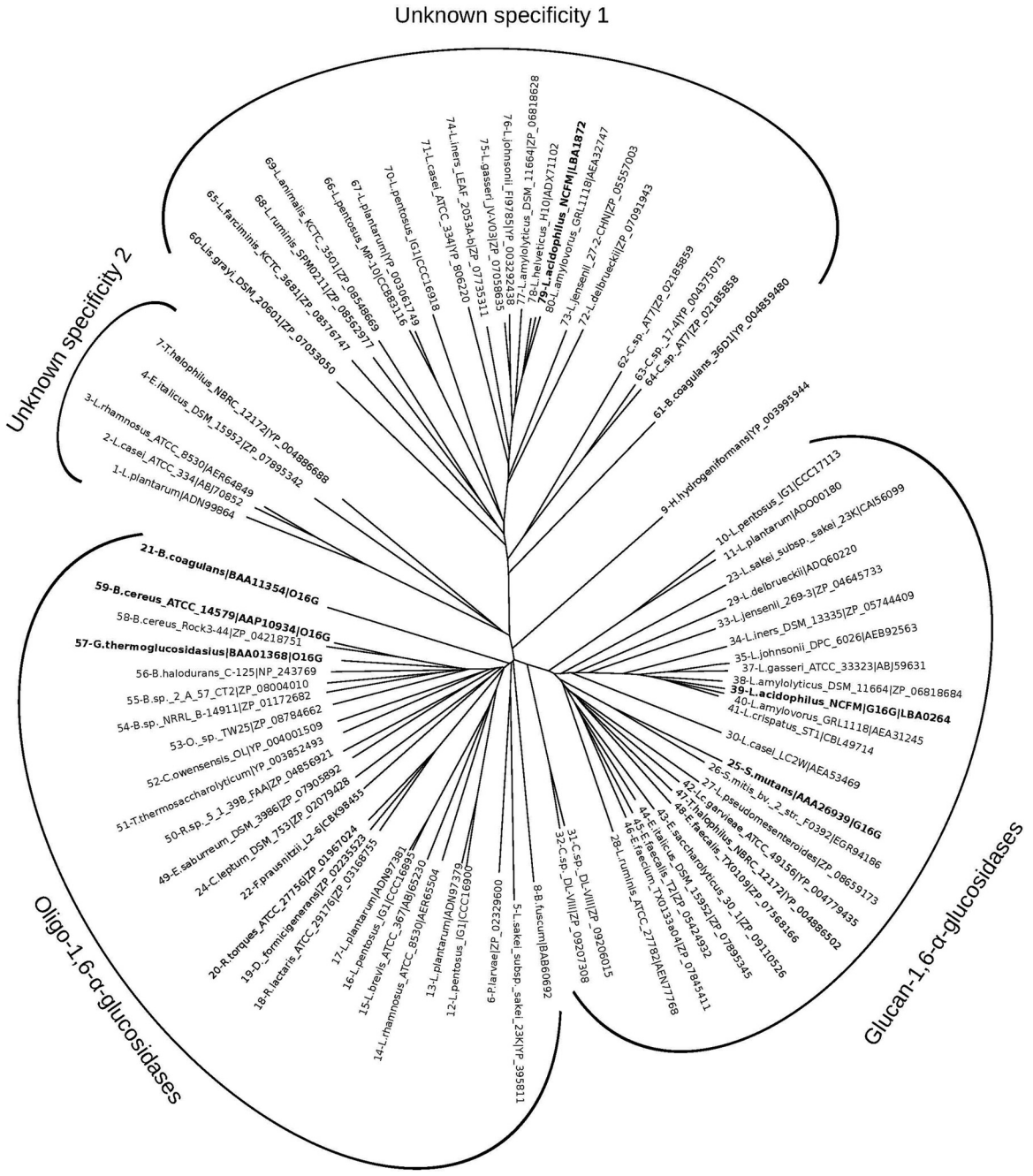

FIG 2 Phylogenetic tree constructed based on the multiple sequence alignment partly shown in Fig. 1 (full alignment is shown in Fig. S1 in the supplemental material). The tree depicts the clustering of three main groups of GH13 enzymes: (i) a glucan 1,6-α-glucosidase (G16G) cluster from mainly acidophilus complex lactobacilli including *La*GH13_31, streptococci, enterococci, and others (see Table S3); (ii) an oligo-1,6-α-glucosidase (O16G) cluster containing characterized enzymes from bacilli, together with a variety of uncharacterized sequences from other Gram-positive bacteria including a branch of non-acidophilus complex lactobacilli; (iii) a cluster of uncharacterized sequences homologous to LBA1872 that occurs in the maltooligosaccharide operon in *L. acidophilus* NCFM and forms a distinct group (Unknown specificity 1), supportive of the lack of α-1,6 sequence motifs and suggestive of a different function. A small group of uncharacterized sequences form a fourth intermediate group (Unknown specificity 2), whereas a single sequence resembling possibly an ancestral O16G segregates alone, likely due to its taxonomic distance to other O16G sequences in the tree. The following *Lactobacillus* species are represented: *L. amylolyticus*, *L. animalis*, *L. brevis*, *L. delbrueckii*, *L. farciminis*, *L. jensenii*, *L. helveticus*, *L. iners*, *L. pentosus*, *L. plantarum*, *L. rhamnosus*, *L. ruminis*, and *L. sakei* subsp. *sakei*. Other species are as follows: *B. halodurans*, *Bacillus halodurans*; *B.* sp. 2_A_57_CT2, *Bacillus* sp. strain 2_A_57_CT2; *B.* sp. NRRL B-14911, *Bacillus* sp. strain NRRL B-14911; *B. fuscum*, *Brevibacterium fuscum*; *L. garvieae*, *Lactococcus garvieae*; *C.* sp. AT7, *Carnobacterium* sp. strain AT7; *C.* sp. 17-4, *Carnobacterium* sp. strain 17-4; *C.* sp. DL-VIII, *Clostridium* sp. strain DL-VIII; *C. leptum*, *Clostridium leptum*; *C. owensensis*, *Caldicellulosiruptor owensensis*; *D. formicigenerans*, *Dorea formicigenerans*; *E. saccharolyticus*, *Enterococcus saccharolyticus*; *E. faecium*, *Enterococcus faecium*; *E. italicus*, *Enterococcus italicus*; *E. saburreum*, *Eubacterium saburreum*; *F. prausnitzii*, *Faecalibacterium prausnitzii*; *H. hydrogeniformans*, *Halanaerobium hydrogeniformans*; *Lis. grayi*, *Listeria grayi*; *L. pseudomesenteroides*, *Leuconostoc pseudomesenteroides*; *O.* sp. TW25, *Ornithinibacillus* sp. strain TW25; *P. larvae*, *Paenibacillus larvae*; *R.* sp. 5_1_39B_FAA, *Ruminococcus* sp. strain 5_1_39B_FAA; *R. lactaris*, *Ruminococcus lactaris*; *R. torques*, *Ruminococcus torques*; *S. mitis*, *Streptococcus mitis*; *T. halophilus*, *Tetragenococcus halophilus*; *T. thermosaccharolyticum*, *Thermoanaerobacterium thermosaccharolyticum*. Other species are as identified in the text.

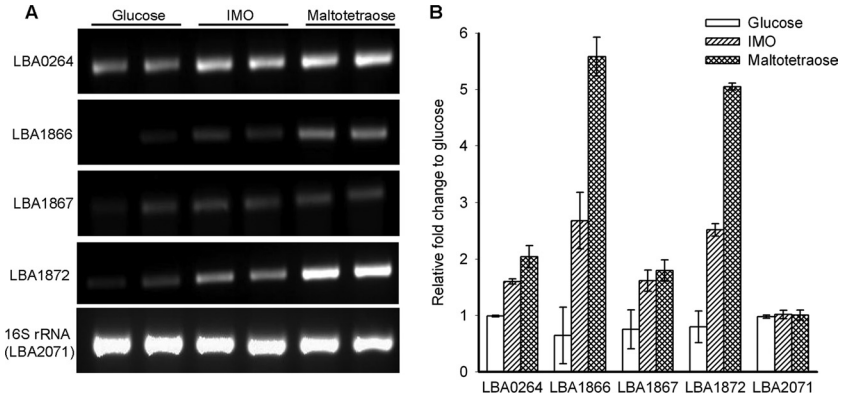

FIG 3 (A) The semiquantitative RT-PCR amplified fragments at the end of 22 cycles of selected genes of *L. acidophilus* NCFM grown in duplicates on semiessential medium with 1% glucose, isomaltooligosaccharides (IMO), and maltotetraose. PCR products were separated by agarose electrophoresis and quantified by densitometry. (B) The levels of gene transcripts were quantified as the ratio of intensity of IMO and maltotetraose to the intensity of glucose-grown cultures. The expression of the 16S rRNA gene was used as an internal control. LBA0264, glucan 1,6-α-glucosidase; LBA1866, maltose ABC transporter permease protein; LBA1867, multiple sugar binding ABC transporter system; LBA1872, GH13 of unknown function; LBA2071, 16S rRNA gene.

geneity, and its pI was determined to be 4.8 in accordance with the theoretically calculated value of 4.9. The yield of *La*GH13_31 after two purification steps was 25 mg/liter of culture with a specific activity of 335 U/mg. The pH optimum for *La*GH13_31 was determined to be 5.5, and the enzyme retained more than 50% of its maximum activity at pH 4 to 8 (see Fig. S2A in the supplemental material). The temperature optimum at pH 6 was 39°C (see Fig. S2B), and the inactivation rate constants at 37°C and 50°C were 0.001 min^{-1} and 0.0152 min^{-1}, respectively, corresponding to a $t_{1/2}$ of 4.8 days and 46 min, respectively.

Substrate preference. The substrate specificity of *La*GH13_31 was investigated by measuring initial reaction rates for eight substrates (1 mM) (Table 3) including IMO (DP 2 to 4), panose that has an α-1,6 linkage, sucrose, and disaccharides containing α-1,1- or α-1,4-linked glucose. Among the natural substrates, the highest rate of hydrolysis was on panose (Table 3), and *La*GH13_31 clearly preferred IMO longer than IG2, while having negligible activity on other natural substrates, confirming its function as a glucan 1,6-α-glucosidase.

Kinetic analysis performed on IMO and dextran confirmed this trend and showed higher catalytic efficiencies (k_{cat}/K_m) of *La*GH13_31 on IG3 and IG4 than isomaltose (Table 4). Although saturation was not reached at the highest dextran concentration used (40 mg/ml), clear curvature of the Michaelis-Menten plot (see Fig. S3 in the supplemental material) allowed unambiguous determination of the kinetic parameters.

Effective inhibition by the product glucose indicates possible feedback regulation of the activity of *La*GH13_31. The Michaelis-Menten plots of PNPG hydrolysis showed significant inhibition by 6 or 8 mM glucose (see Fig. S4 in the supplemental material). The competitive inhibition model gave the best fits to the data ($R^2 = 0.999$), and the K_i of glucose was determined to 4.0 ± 0.18 mM.

Three-dimensional structure of *La*GH13_31. Obtained crystals of *La*GH13_31 belonged to space group $P2_12_12$ with one monomer in the asymmetric unit. The crystals diffracted to 2.05-Å resolution, and the structure was solved by molecular replacement using the structure of *Sm*GH13_31 (PDB 2ZIC). The overall structure of *La*GH13_31 (Fig. 4) shows the classical GH13 architecture of a catalytic $(\beta/\alpha)_8$-barrel fold domain (domain A) and a C-terminal antiparallel β-sheet domain (domain C). The three catalytic residues conserved in GH13 are situated at the ends of β-strands 4 (Asp198, catalytic nucleophile), 5 (Glu240, catalytic acid-base), and 7 (Asp316, transition state stabilizer). Functionally important amino acid residues at the active-site substrate binding subsites −1 through to +2 are depicted in Fig. 5A, following the accepted subsite nomenclature, with the minus subsites at the nonreducing end of the substrate and plus subsites at the reducing end and hydrolysis occurring between the −1 and +1 subsites (10). Domain A, comprising the first 465 residues of

TABLE 3 Normalized reaction rate of *La*GH13_31 on various substrates

Substrate[a]	Reaction rate (s^{-1})[b]	Relative rate (%)[c]
PNPG	164.0 ± 5.1	94.3
IG2	26.6 ± 1.3	15.3
IG3	41.2 ± 0.9	23.7
IG4	41.0 ± 0.2	23.6
Trehalose	ND[d]	
Maltose	$(4.9 \pm 0.2) \times 10^{-2}$	0.03
Sucrose	$(10.5 \pm 1.5) \times 10^{-2}$	0.06
Panose	173.9 ± 2.4	100

[a] Substrates were used at a concentration of 1 mM.
[b] The reaction rate was calculated as $V/[E]$, where V is the initial velocity and $[E]$ is the enzyme concentration.
[c] Relative to the reaction rate toward panose.
[d] ND, not detected.

TABLE 4 Kinetic parameters of *La*GH13_31 at 37°C and pH 6.0

Substrate	k_{cat} (s^{-1})	K_m (mM)	k_{cat}/K_m (s^{-1} mM^{-1})	Relative k_{cat}/K_m[a]
IG2	517 ± 6.3	22.5 ± 0.7	23	14.6
IG3	475 ± 12.7	14.1 ± 0.8	34	21.7
IG4	501 ± 12.7	16.1 ± 0.9	31	19.7
PNPG	597 ± 14.3	2.38 ± 0.16	251	159.9
Panose	612 ± 12.8	3.9 ± 0.2	157	100
Dextran	384 ± 17.1	29.2 ± 2.4[b]	13.6[c]	8.7

[a] Normalized to panose.
[b] mg ml^{-1}.
[c] s^{-1} mg^{-1} ml.

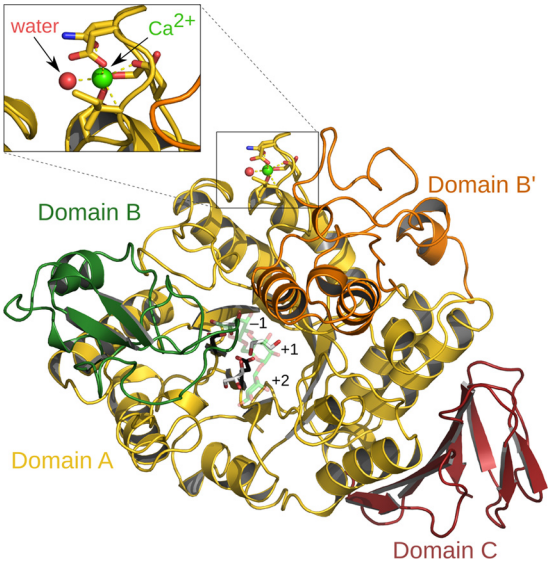

FIG 4 Crystal structure of *La*GH13_31. Domain A (residues 3 to 100, 170 to 358, and 445 to 465) is shown in yellow, domain B (residues 101 to 169) is in green, domain B′ (residues 359 to 444) is in orange, and domain C (residues 466 to 538) is in red. The catalytic residues (Asp198 and Glu240) are shown as black sticks, and three glycerol molecules in the active site are shown with white carbons. An IG3 molecule from *Sm*GH13_31 (2ZID) is superimposed and shown with green carbons at 60% transparency. A calcium ion (green sphere) is coordinated by a water molecule (red sphere) and residues 20, 22, 24, 26, and 28, and a close-up view of the Ca^{2+} binding site is shown for clarity.

*La*GH13_31, contains two inserts after the fourth and eighth β-strands. The first insert is referred to as domain B (residues 101 to 169) and provides residues responsible for substrate recognition. Domain B′ (residues 359 to 444), the second insert, has residues interacting with the substrate and domain B. Overall, these inserts render the active site less accessible. Domain C (residues 466 to 539) assumes a β-sandwich fold composed of five strands packing against domain A and two shorter β-strands that are solvent exposed.

A Ca^{2+} is bound in domain A in a loop located just before the first helix in a binding site resembling that observed in *Sm*GH13_31 (19). The Ca^{2+} octahedral coordination shell comprises the side chains of Asp20, Asn22, Asp24, and Asp28, the carbonyl oxygen of Ile26, and a water molecule. The protein ligands are well conserved within GH13_31, suggesting the recurrence of the Ca^{2+} binding site within this group of enzymes. The structure of the O16G from *B. cereus* (*Bc*O16G) has no Ca^{2+} at this site (56), possibly because the crystallization conditions included 5 mM EDTA. For *La*GH13_31, adding EDTA to the crystallization conditions abolished crystal formation, and recently it has been shown that the presence of Ca^{2+} enhances the thermostability of *Sm*GH13_31 (26), supporting a structural role of this divalent ion in GH13_31. Interestingly, the water path between the active site and the surface of the enzyme, which was suggested to have functional significance as a water drain in *Sm*GH13_31 (19), is also conserved in *La*GH13_31 (see Fig. S5 in the supplemental material).

In addition to structurally ordered water molecules, the electron density revealed the presence of three MES (only the sulfonic acid moiety of MES A 1547 is modeled) and eight glycerol molecules. One of the MES molecules was bound by Tyr150 and Tyr157, also present in *Sm*GH13_31 (Tyr146 and Tyr153) and *Bc*O16G (Tyr151 and Tyr158). Three of the glycerol molecules were found in the active site, and comparison with the *Sm*GH13_31 in complex with isomaltotriose revealed that glycerol 1542 together with waters 2215, 2249, and 2334 are ligands to the same residues as observed at the −1 subsite in *Sm*GH13_31, thus demonstrating the conservation of this pivotal subsite (Fig. 5).

DISCUSSION

The administration of IMO has been reported to result in an increase in bifidobacteria and lactobacilli in humans and rats (23,

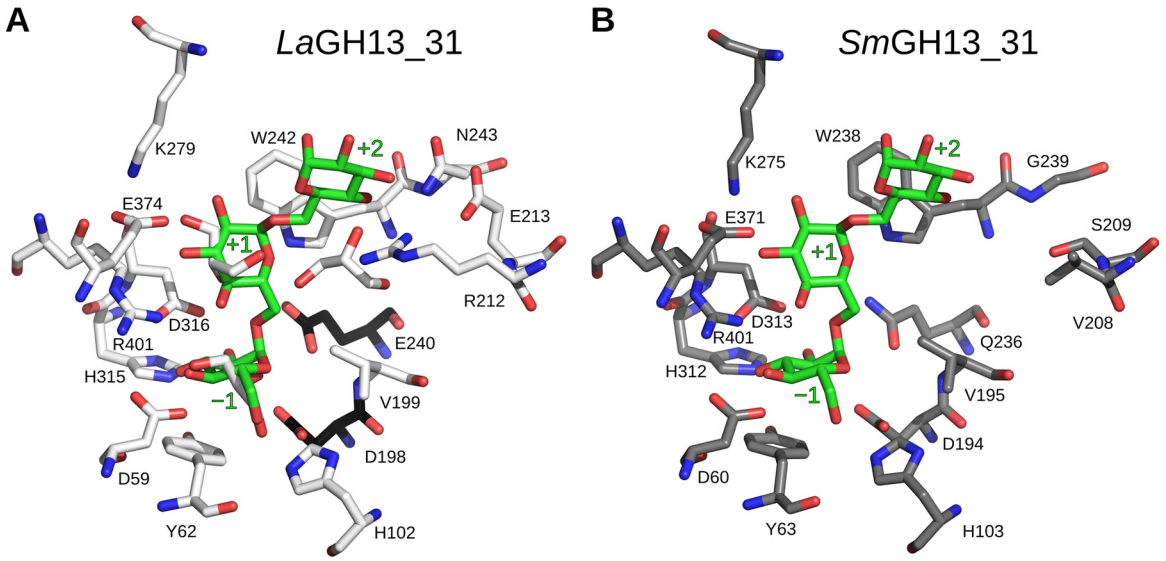

FIG 5 Close-up view of the residues comprising the active sites of *La*GH13_31 (white carbon atoms) (A) and *Sm*GH13_31, (gray carbon atoms) (B). The catalytic residues from *La*GH13_31 are black, and the green IG3 molecule in panels A and B originates from *Sm*GH13_31 (Glu236Gln inactive mutant; PDB 2ZID) and denotes the substrate binding subsites −1, +1, and +2. The largest difference is seen near the +2 subsite.

25). This was recently corroborated by a human intervention study showing a significant increase of bifidobacteria and lactobacilli, together with a 3-fold decrease in clostridia, due to IMO administration in elderly constipated humans, highlighting the selectivity of IMO (58). Surprisingly, the genetics and enzymology of IMO utilization remain unexplored in the gut niche. The present study investigates the genetic basis and the enzymology of IMO utilization in *L. acidophilus* NCFM, which serves as a model for probiotic lactobacilli.

Bioinformatic analysis. A single gene encoding a GH13_31 enzyme (LBA0264, designated *La*GH13_31) was found in the *L. acidophilus* NCFM genome. In addition, a putative enzyme, encoded by the locus LBA1872, displayed low similarity to O16Gs. *La*GH13_31 is homologous to the characterized *Sm*GH13_31 (Table 2), as evident from the multiple sequence alignment (Fig. 1) and the phylogenetic tree that depicts the clustering of *La*GH13_31 and closely related enzymes mainly from the acidophilus complex lactobacilli together with the G16G from *S. mutans* (Fig. 2; see also Table S3 in the supplemental material). Characterized GH13_31 O16G from different bacilli formed an adjacent cluster (Fig. 2). Interestingly, although this O16G cluster contained sequences from lactobacilli, none of these belonged to the acidophilus complex (see Table S3), suggesting that the gut niche adaptation has driven the enrichment of the G16G specificity in acidophilus complex *Lactobacillus* members and/or that shorter IMO are catabolized using different enzymes in acidophilus complex members. Furthermore, *La*GH13_31 contained both the QPDLN motif in the conserved region V of the α-amylase family, reported to define the O16G subfamily containing both O16G and G16G (38), and the shorter β→α loop 4 that distinguishes G16G from O16G (43). Taken together, this strongly suggested that *La*GH13_31 is a G16G. In contrast, LBA1872 was clearly distinguishable from characterized enzymes with O16G, and its amino acid sequence resembled the intermediate group having a region V MPKLN motif and a conserved histidine in region II (Fig. 1) (38). More importantly, the valine residue following the catalytic nucleophile, which was experimentally identified as a key signature of α-1,6 hydrolytic activity (57), is instead an alanine (shown in boldface) in LBA1872 (GLRLD**A**;region II). This, together with the segregation of LBA1872 with other homologues from mainly the *Lactobacillus* genus in a separate cluster (Fig. 2, Unknown specificity 1), is indicative of a different specificity of this group of enzymes tentatively annotated as O16Gs in the NCBI database based exclusively on *in silico* predictions.

Genetics of IMO utilization in *L. acidophilus* and other gut bacteria. The organization of genes mediating utilization of FOS and raffinose oligosaccharides in functional operons comprising transport systems, hydrolases, and transcriptional regulators has been reported in *L. acidophilus* NCFM (5, 6). Interestingly, LBA1872 is located within the maltooligosaccharide utilization operon, which also encodes a complete ABC transport system annotated as a maltose/maltooligosaccharide transporter, a LacI transcriptional regulator, a GH65 maltose phosphorylase (EC 2.4.1.8), and a GH13_20 maltogenic α-amylase (EC 3.2.1.133). GH13_20 enzymes also possess neopullulanase activity (EC 3.2.1.135) and are typically annotated as neopullulanases (34) (Fig. 6A). This organization is also observed in other *L. acidophilus* strains (e.g., *L. acidophilus* ATCC 4796) and in closely related acidophilus complex species, e.g., *Lactobacillus amylovorus* GRL1118 and *Lactobacillus crispatus* ST1 (Fig. 6B and C). Another similarity between *L. acidophilus* NCFM and the aforementioned organisms is that genes encoding GH13_31 enzymes which confer IMO hydrolysis are not in proximity to carbohydrate hydrolysis or transport loci (Fig. 6A to C). In contrast, the GH13_31-encoding genes are located in the maltooligosaccharide operon in other species of the acidophilus complex represented by *Lactobacillus johnsonii* ATCC 33200 and *Lactobacillus gasseri* JV-V03 (Fig. 6D and E) as well as in other *Lactobacillus* species, e.g., *Lactobacillus casei* BL23 (Fig. 6F), and in *S. mutans* (data not shown), suggesting that the relocation of the GH13_31 genes in *L. acidophilus* NCFM and closely related organisms is a recent evolutionary event. With respect to IMO transport, the presence of GH13_31-encoding genes in maltooligosaccharide operons in several lactobacilli, including many acidophilus complex members, suggests that IMO may be internalized by the ABC transporters present in these operons. It is unclear if the same is valid for the group represented by *L. acidophilus* NCFM, where the GH13_31 resides on a separate locus. It cannot be ruled out, however, that uptake of a shorter IMO, e.g., IG2, occurs via other types of transporters, e.g., phosphoenolpyruvate-dependent phosphotransferase system (PTS), as demonstrated in the case of maltose/maltooligosaccharide utilization in other Gram-positive bacteria, where maltose is internalized via a PTS transporter and where longer maltooligosaccharides are transported via an ABC transporter (1, 45). Phosphorylated maltose and maltotriose internalized via a PTS are recognized by a specific GH4 6-phospho-α-glucosidase (EC 3.2.1.122) (45). Noticeably, GH4-encoding genes occur frequently in acidophilus complex lactobacilli including *L. acidophilus* NCFM (LBA1689).

Bifidobacteria encode GH13 α-glucosidases that are distantly related to GH13_31 but resemble GH13_31 O16Gs with respect to activity on shorter IMO (39, 52) and have the important Val residue following the nucleophile, consistent with α-1,6 activity. Genes encoding GH13_31 enzymes are also present in enterococci, e.g., *Enterococcus faecalis* OG1RF (Fig. 6G). On the other hand, commensals from the genus *Bacteroides* lack GH13_31 enzymes. Only three gut-adapted *Clostridia difficile* strains possess putative GH13_31 enzymes. The specificity of these putative enzymes toward IMO has not been demonstrated, and a closer analysis showed that they lack the valine residue presented above as an important α-1,6 specificity signature. This is consistent with the observed selectivity of IMO on human gut microbiota, manifested in a 3-fold reduction in clostridia counts following IMO intake (58).

The present transcriptional analysis suggests that IMO induce the expression of LBA0264 and the ABC transport systems as well as LBA1872 in the maltooligosaccharide gene cluster. Remarkably, the same loci are also induced by maltotetraose, suggesting coregulation of genes associated with utilization of α-1,4- and α-1,6-glucooligosaccharides. The inducer of the maltose/maltooligosaccharide operon in *Streptococcus pneumoniae* (belongs to the same order as lactobacilli) has been identified as maltose (36). This disaccharide is the product of panose (abundant in commercial IMO preparations) hydrolysis by *La*GH13_31-like enzymes or is the product of maltooligosaccharide hydrolysis by GH13_20 maltogenic α-amylases (EC 3.2.1.133) encoded within the maltooligosaccharide operon discussed above (Fig. 6A). Thus, maltose is a common degradation product of the panose fraction of IMO and maltooligosaccharides, which provides a possible rationale for the coregulation and the colocalization of hydrolases of these two pathways in some acidophilus complex members.

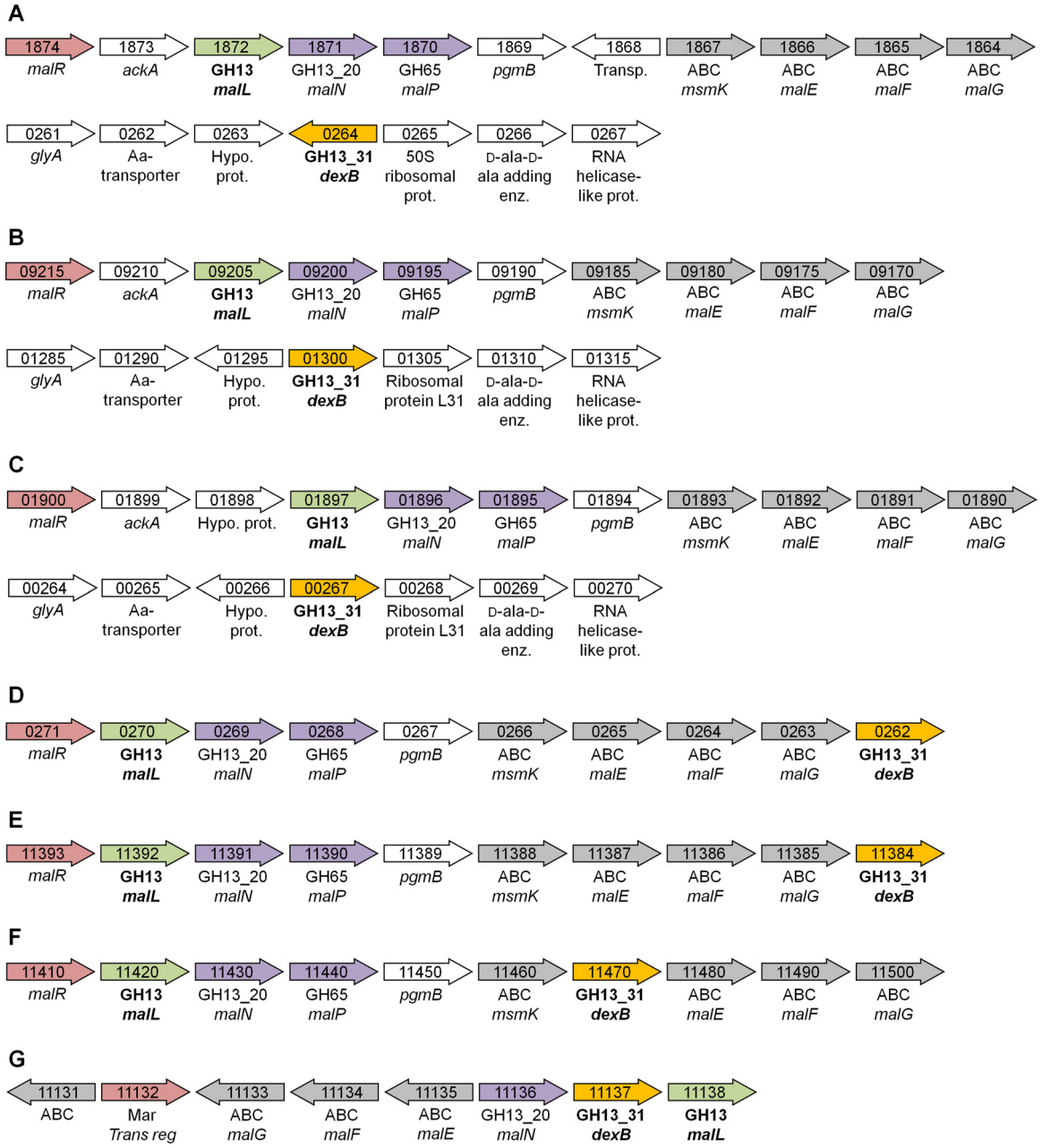

FIG 6 Schematic presentation of the gene organization around G16Gs (yellow) and LBA1872-like GH13 genes (green) from different organisms. Transcriptional regulators are represented in red, and glycoside hydrolases are shown in purple. ABC (gray) refers to proteins, which are a part of an ABC transport system. Numbers in the arrows refers to locus tag numbers. (A) *Lactobacillus acidophilus* NCFM. (B) *L. amylovorus* GRL1118. (C) *L. crispatus* ST1. (D) *L. johnsonii* ATCC 33200. (E) *L. gasseri* JV-V03. (F) *L. casei* BL23. (G) *Enterococcus faecalis* OG1RF. The information in the figure is derived from the genome database provided by NCBI, and in the case of *L. acidophilus* NCFM and *L. casei* BL23, information is based on previous studies (33, 34).

Activity and structure of *La*GH13_31. The activity profile of *La*GH13_31 confirmed the bioinformatic analysis predicting its G16G specificity. Interestingly, this enzyme displays a 43-fold higher dextran/panose catalytic efficiency ratio (Table 4) than *Sm*GH13_31 (43). This suggests higher affinity in the distal aglycone substrate subsites of the active-site cleft of *La*GH13_31. A structural alignment of *La*GH13_31 and *Sm*GH13_31 indicates similar binding modes at the −1 and +1 subsites but large differences at subsite +2, where the residues Arg212, Glu213, and Asn243 in *La*GH13_31 correspond to Val208, Ser209, and Gly239, respectively, in *Sm*GH13_31 (Fig. 5). Superposing the two structures (using superpose in COOT [13]) shows that Arg212 NH1 is 2.9 Å from Glc-879 O3 (glucosyl moiety at subsite +2) and that Asn243 OD1 is 2.8 Å from Glc-879 O4 at the +2 subsite (Fig. 5), thus supporting a larger number of interactions at subsite +2 in *La*GH13_31 relative to *Sm*GH13_31. It is intriguing that additional interactions at subsite +2 would have this profound effect on the activity on dextran. One hypothesis is that these additional

contacts at subsite +2 result in better anchoring of the substrate polysaccharide chain, which can act in concert with weak surface binding sites to elicit the observed difference. This synergy between the active site and surface binding sites has been reported in other GH13 enzymes (35) but remains currently unidentified in GH13_31. The conservation of some aromatic residues on the surface of GH13_31 enzymes, e.g., Tyr150 and Tyr157 in *La*GH13_31, merits further studies to assess their role in activity on polymeric substrates.

Product inhibition by glucose seems to be relevant for the regulation of *La*GH13_31 activity as the measured K_i for glucose (4 mM) is in the same range or lower than the K_m for both natural and synthetic substrates (Table 4). This inhibition has not been shown for GH13_31 enzymes displaying G16G specificity, but it was reported for the O16G from *B. coagulans*, albeit slightly less effectively (K_i/K_m ratio of 4.7 compared to 1.7 for *La*GH13_31) (47).

Conclusions. Genomes of probiotic lactobacilli from the acidophilus complex consistently encode glucan 1,6-α-glucosidase genes located either in a maltooligosaccharide operon encompassing an ABC transport system and maltooligosaccharide active enzymes, as in *L. johnsonii* and *L. gasseri* members, or located on separate loci, as in *L. acidophilus* NCFM and closely related species and strains. Similar transcriptional regulation of the GH13_31-encoding gene and genes in the maltooligosaccharide operon including the ABC transporter suggests that the pathways for α-1,4 and α-1,6 glucan catabolism are linked, possibly through maltose, which is a common hydrolysis product. Bioinformatic analysis of one of the conserved GH13 α-glucan operon genes (LBA1872 in *L. acidophilus* NCFM) showed that this gene is most probably misannotated as an O16G as it lacks motif signatures shown to be pivotal for α-1,6 activity and as it segregates in a separate cluster from canonical GH13_31 IMO active enzymes. In contrast, the recombinant *La*GH13_31 was shown to be an active glucan 1,6-α-glucosidase catalyzing hydrolysis of longer IMO and product-inhibited by glucose. The crystallographic structure of *La*GH13_31 shows a conserved subsite −1 but several additional substrate contacts at subsite +2 compared to related enzymes, which may explain the high affinity of this enzyme for dextran.

ACKNOWLEDGMENTS

Mette Pries is acknowledged for technical assistance and Anne Blicher for performing the amino acid analysis. Haruhide Mori from Hokkaido University is acknowledged for valuable discussions on the determinants of 1,6-α-glucosidase activity. Joakim Mark Andersen is acknowledged for discussion on the genetics of lactic acid bacteria. Dorthe Boelskifte (University of Copenhagen) is acknowledged for help with crystallization. MAX-lab and MAX-lab staff are thanked for beam time and assistance as well as the DANSCATT program from the Danish National Research Council for travel support.

This work was supported by a grant from the Danish Strategic Research Council, Committee of Health and Nutrition, to the project Gene Discovery and Molecular Interactions in Prebiotics/Probiotics Systems: Focus on Carbohydrate Prebiotics.

REFERENCES

1. **Abbott DW, et al.** 2010. The molecular basis of glycogen breakdown and transport in *Streptococcus pneumoniae*. Mol. Microbiol. **77**:183–199.
2. **Afonine P, Grosse-Kunstleve R, Adams P.** 2005. A robust bulk-solvent correction and anisotropic scaling procedure. Acta Crystallogr. D Biol. Crystallogr. **61**:850–855.
3. **Altermann E, et al.** 2005. Complete genome sequence of the probiotic lactic acid bacterium *Lactobacillus acidophilus* NCFM. Proc. Natl. Acad. Sci. U. S. A. **102**:3906–3912.
4. **Barkholt V, Jensen AL.** 1989. Amino-acid analysis—determination of cysteine plus half-cystine in proteins after hydrochloric-acid hydrolysis with a disulfide compound as additive. Anal. Biochem. **177**:318–322.
5. **Barrangou R, Altermann E, Hutkins R, Cano R, Klaenhammer TR.** 2003. Functional and comparative genomic analyses of an operon involved in fructooligosaccharide utilization by *Lactobacillus acidophilus*. Proc. Natl. Acad. Sci. U. S. A. **100**:8957–8962.
6. **Barrangou R, et al.** 2006. Global analysis of carbohydrate utilization by *Lactobacillus acidophilus* using cDNA microarrays. Proc. Natl. Acad. Sci. U. S. A. **103**:3816–3821.
7. **Britton HTS, Robinson RA.** 1931. Universal buffer solutions and the dissociation constant of veronal. J. Chem. Soc. **1931**:1456–1462.
8. **Cantarel BL, et al.** 2009. The Carbohydrate-Active EnZymes database (CAZy): an expert resource for glycogenomics. Nucleic Acids Res. **37**: D233–D238.
9. **Chen VB, et al.** 2010. MolProbity: all-atom structure validation for macromolecular crystallography. Acta Crystallogr. D Biol. Crystallogr. **66**:12–21.
10. **Davies G, Wilson K, Henrissat B.** 1997. Nomenclature for sugar-binding subsites in glycosyl hydrolases. Biochem. J. **321**:557–559.
11. **de Vrese M, Schrezenmeir J.** 2008. Probiotics, prebiotics, and synbiotics. Adv. Biochem. Eng. Biotechnol. **111**:1–66.
12. **Edgar RC.** 2004. MUSCLE: multiple sequence alignment with high accuracy and high throughput. Nucleic Acids Res. **32**:1792–1797.
13. **Emsley P, Lohkamp B, Scott WG, Cowtan K.** 2010. Features and development of Coot. Acta Crystallogr. D Biol. Crystallogr. **66**:486–501.
14. **Fredslund F, et al.** 2011. Crystal Structure of α-galactosidase from *Lactobacillus acidophilus* NCFM: insight into tetramer formation and substrate binding. J. Mol. Biol. **412**:466–480.
15. **Fukuda S, et al.** 2011. Bifidobacteria can protect from enteropathogenic infection through production of acetate. Nature **469**:543–547.
16. **Gilliland SE, Speck ML, Morgan CG.** 1975. Detection of *Lactobacillus acidophilus* in aeces of humans, pigs, and chickens. Appl. Microbiol. **30**: 541–545.
17. **Goffin D, et al.** 2011. Will isomalto-oligosaccharides, a well-established functional food in Asia, break through the European and American market? The status of knowledge on these prebiotics. Crit. Rev. Food Sci. Nutr. **51**:394–409.
18. **Gotsche S, Dahl MK.** 1995. Purification and characterization of the phospho-α(1,1)glucosidase (TreA) of *Bacillus subtilis* 168. J. Bacteriol. **177**: 2721–2726.
19. **Hondoh H, et al.** 2008. Substrate recognition mechanism of α-1,6-glucosidic linkage hydrolyzing enzyme, dextran glucosidase from *Streptococcus mutans*. J. Mol. Biol. **378**:913–922.
20. **Huson DH, et al.** 2007. Dendroscope: An interactive viewer for large phylogenetic trees. BMC Bioinformatics **8**:460. doi:10.1186/1471-2105-8-460.
21. **Kabsch W.** 2010. Xds. Acta Crystallogr. D Biol. Crystallogr. **66**:125–132.
22. **Kaneko T, Yokoyama A, Suzuki M.** 1995. Digestibility characteristics of isomaltooligosaccharides in comparison with several saccharides using the rat jejunum loop method. Biosci. Biotechnol. Biochem. **59**:1190–1194.
23. **Kaneko T, et al.** 1994. Effects of isomaltooligosaccharides with different degrees of polymerization on human fecal bifidobacteria. Biosci. Biotechnol. Biochem. **58**:2288–2290.
24. **Kano T, Usami Y, Adachi T, Tatematsu M, Hirano K.** 1996. Inhibition of purified human sucrase and isomaltase by ethanolamine derivatives. Biol. Pharm. Bull. **19**:341–344.
25. **Ketabi A, Dieleman LA, Gaenzle MG.** 2011. Influence of isomalto-oligosaccharides on intestinal microbiota in rats. J. Appl. Microbiol. **110**: 1297–1306.
26. **Kobayashi M, et al.** 2011. Calcium ion-dependent increase in thermostability of dextran glucosidase from *Streptococcus mutans*. Biosci. Biotechnol. Biochem. **75**:1557–1563.
27. **Larkin MA, et al.** 2007. Clustal W and Clustal X version 2.0. Bioinformatics **23**:2947–2948.
28. **Lebeer S, Vanderleyden J, De Keersmaecker SCJ.** 2008. Genes and molecules of lactobacilli supporting probiotic action. Microbiol. Mol. Biol. Rev. **72**:728–764.
29. **Macfarlane S, Macfarlane GT, Cummings JH.** 2006. Review article:

prebiotics in the gastrointestinal tract. Aliment. Pharmacol. Ther. **24**:701–714.
30. **MacGregor EA, Janecek S, Svensson B.** 2001. Relationship of sequence and structure to specificity in the α-amylase family of enzymes. Biochim. Biophys. Acta **1546**:1–20.
31. **Majumder A, et al.** 2011. Proteome reference map of *Lactobacillus acidophilus* NCFM and quantitative proteomics towards understanding the prebiotic action of lactitol. Proteomics **11**:3470–3481.
32. **Makelainen H, Hasselwander O, Rautonen N, Ouwehand AC.** 2009. Panose, a new prebiotic candidate. Lett. Appl. Microbiol. **49**:666–672.
33. **Monedero V, Yebra MJ, Poncet S, Deutscher J.** 2008. Maltose transport in *Lactobacillus casei* and its regulation by inducer exclusion. Res. Microbiol. **159**:94–102.
34. **Nakai H, et al.** 2009. The maltodextrin transport system and metabolism in *Lactobacillus acidophilus* NCFM and production of novel α-glucosides through reverse phosphorolysis by maltose phosphorylase. FEBS J. **276**: 7353–7365.
35. **Nielsen MM, et al.** 2009. Two secondary carbohydrate binding sites on the surface of barley α-amylase 1 have distinct functions and display synergy in hydrolysis of starch granules. Biochemistry **48**:7686–7697.
36. **Nieto C, Espinosa M, Puyet A.** 1997. The maltose/maltodextrin regulon of *Streptococcus pneumoniae*: differential promoter regulation by the transcriptional repressor MalR. J. Biol. Chem. **272**:30860–30865.
37. **O'Flaherty S, Klaenhammer TR.** 2010. The role and potential of probiotic bacteria in the gut, and the communication between gut microflora and gut/host. Int. Dairy J. **20**:262–268.
38. **Oslancova A, Janecek S.** 2002. Oligo-1,6-glucosidase and neopullulanase enzyme subfamilies from the α-amylase family defined by the fifth conserved sequence region. Cell. Mol. Life Sci. **59**:1945–1959.
39. **Pokusaeva K, O'Connell-Motherway M, Zomer A, Fitzgerald GF, van Sinderen D.** 2009. Characterization of two novel α-glucosidases from *Bifidobacterium breve* UCC2003. Appl. Environ. Microbiol. **75**:1135–1143.
40. **Rice P, Longden I, Bleasby A.** 2000. EMBOSS: The European molecular biology open software suite. Trends Genet. **16**:276–277.
41. **Rimmele M, Boos W.** 1994. Trehalose-6-phosphate hydrolase of *Escherichia coli*. J. Bacteriol. **176**:5654–5664.
42. **Saburi W, et al.** 2008. Structure-function relationship of substrate length specificity of dextran glucosidase from *Streptococcus mutans*. Biologia **63**: 1000–1005.
43. **Saburi W, Mori H, Saito S, Okuyama M, Kimura A.** 2006. Structural elements in dextran glucosidase responsible for high specificity to long chain substrate. Biochim. Biophys. Acta **1764**:688–698.
44. **Sanders ME, Klaenhammer TR.** 2001. The scientific basis of *Lactobacillus acidophilus* NCFM functionality as a probiotic. J. Dairy Sci. **84**:319–331.
45. **Schonert S, et al.** 2006. Maltose and maltodextrin utilization by *Bacillus subtilis*. J. Bacteriol. **188**:3911–3922.
46. **Stam MR, Danchin EGJ, Rancurel C, Coutinho PM, Henrissat B.** 2006. Dividing the large glycoside hydrolase family 13 into subfamilies: towards improved functional annotations of α-amylase-related proteins. Protein Eng. Des. Sel. **19**:555–562.
47. **Suzuki Y, Tomura Y.** 1986. Purification and characterization of *Bacillus coagulans* oligo-1,6-glucosidase. Eur. J. Biochem. **158**:77–83.
48. **Suzuki Y, Aoki R, Hayashi H.** 1982. Assignment of a *p*-nitrophenyl-α-D-glucopyranoside-hydrolyzing α-glucosidase of *Bacillus cereus* ATCC 7064 to an exo-oligo-1,6-glucosidase. Biochim. Biophys. Acta **704**:476–483.
49. **Swennen K, Courtin CM, Delcour JA.** 2006. Non-digestible oligosaccharides with prebiotic properties. Crit. Rev. Food Sci. Nutr. **46**:459–471.
50. **Terwilliger TC, et al.** 2008. Iterative model building, structure refinement and density modification with the PHENIX AutoBuild wizard. Acta Crystallogr. D Biol. Crystallogr. **64**:61–69.
51. **Vagin A, Teplyakov A.** 1997. MOLREP: an automated program for molecular replacement. J. Appl. Crystallogr. **30**:1022–1025.
52. **van den Broek LAM, Struijs K, Verdoes JC, Beldman G, Voragen AGJ.** 2003. Cloning and characterization of two α-glucosidases from *Bifidobacterium adolescentis* DSM20083. Appl. Microbiol. Biotechnol. **61**:55–60.
53. **Wallace TC, et al.** 2011. Human gut microbiota and its relationship to health and disease. Nutr. Rev. **69**:392–403.
54. **Watanabe K, Miyake K, Suzuki Y.** 2001. Identification of catalytic and substrate-binding site residues in *Bacillus cereus* ATCC 7064 oligo-1,6-glucosidase. Biosci. Biotechnol. Biochem. **65**:2058–2064.
55. **Watanabe K, Fujiwara H, Inui K, Suzuki Y.** 2002. Oligo-1,6-glucosidase from a thermophile, *Bacillus thermoglucosidasius* KP 1006, was efficiently produced by combinatorial expression of GroEL in *Escherichia coli*. Biotechnol. Appl. Biochem. **35**:35–43.
56. **Watanabe K, Hata Y, Kizaki H, Katsube Y, Suzuki Y.** 1997. The refined crystal structure of *Bacillus cereus* oligo-1,6-glucosidase at 2.0 angstrom resolution: Structural characterization of proline-substitution sites for protein thermostabilization. J. Mol. Biol. **269**:142–153.
57. **Yamamoto K, Nakayama A, Yamamoto Y, Tabata S.** 2004. Val216 decides the substrate specificity of α-glucosidase in *Saccharomyces cerevisiae*. Eur. J. Biochem. **271**:3414–3420.
58. **Yen C, Tseng Y, Kuo Y, Lee M, Chen H.** 2011. Long-term supplementation of isomalto-oligosaccharides improved colonic microflora profile, bowel function, and blood cholesterol levels in constipated elderly people: a placebo-controlled, diet-controlled trial. Nutrition **27**:445–450.